CD1d/TD APCs. The data are consistent with the hypothesis that removal of sugars linked to both the 2′ and 3′ positions of the galactose is required for T cell stimulation (*26*).

We have shown previously that carbohydrate is not required for GSL binding to CD1d (*11*), suggesting that carbohydrate processing is required to permit interaction with the T cell receptor. To test this possibility, we carried out competition studies. Soluble CD1d molecules were briefly preincubated with either ganglioside G_{M1}, which was shown previously to compete for binding of α-GalCer (*11*), or Gal(α1→2)GalCer, before the addition of stimulatory glycolipids. Both G_{M1} and Gal(α1→2)GalCer were effective as competitors (Fig. 4B), indicating that the additional sugar on Gal(α1→2)GalCer does not prevent its binding to CD1d.

Here, we provided a demonstration of a carbohydrate antigen processing pathway. Interestingly, lysosomal hydrolases, previously thought to be solely involved in GSL metabolism (*27*), are responsible for this function. We confirmed that α-Gal A is located in lysosomes in APCs by assay of subcellular fractions with a chromogenic substrate (*28*). Therefore, some of the contents of the lysosome must have access to CD1d molecules, consistent with the presence of CD1d in lysosomes demonstrated here.

Carbohydrate antigen processing illustrates the ability of antigen presentation systems to co-opt metabolic pathways that have evolved for different purposes. The ability to process carbohydrate antigens could greatly extend the range of antigens that are presented by CD1 molecules. Furthermore, T cell antigen recognition of glycopeptides presented by classical class I and class II molecules is known (*29*), and the carbohydrate linkages in glycopeptides also may be subject to the types of processing events described here.

References and Notes

1. K. L. Rock, A. Goldberg, *Annu. Rev. Immunol.* **17**, 739 (1999).
2. J. A. Villadangos, H. L. Ploegh, *Immunity* **12**, 233 (2000).
3. E. M. Beckman *et al.*, *Nature* **372**, 691 (1994).
4. P. A. Sieling *et al.*, *Science* **269**, 227 (1995).
5. J. E. Gumperz *et al.*, *Immunity* **12**, 211 (2000).
6. A. Shamshiev *et al.*, *Immunity* **13**, 255 (2000).
7. A. Bendelac *et al.*, *Annu. Rev. Immunol.* **15**, 535 (1997).
8. T. Natori *et al.*, *Tetrahedron* **50**, 2771 (1994).
9. T. Kawano *et al.*, *Science* **278**, 1626 (1997).
10. N. Burdin *et al.*, *J. Immunol.* **161**, 3271 (1998).
11. O. Naidenko *et al.*, *J. Exp. Med.* **190**, 1069 (1999).
12. Cell-free antigen presentation assays were performed by coating microwells with 1 μg of soluble CD1d molecules that had been preincubated with antigen. Among the GSL compounds tested, only α-GalCer and Gal(α1→6)GalCer were antigenic in this assay. Competition assays were performed by incubating 2 μg of soluble CD1d protein with a 5-fold molar excess of Gal(α1→2)GalCer or a 10-fold molar excess of G_{M1} gangliosides for 5 min at room temperature before the addition of the vehicle [phosphate-buffered saline (PBS) and 0.05% polysorbate], α-GalCer, or Gal(α1→6)GalCer for an additional 2-hour incubation at 37°C. The wells were then rinsed with PBS and cultured with hybridomas.
13. R. M. Jackman *et al.*, *Immunity* **8**, 341 (1998).
14. V. Briken *et al.*, *J. Exp. Med.* **192**, 281 (2000).
15. APCs were incubated with antigens or the vehicle [dimethyl sulfoxide (DMSO)] for 3 hours at an antigen dose of 50 ng/ml, unless stated otherwise. The antigen-pulsed APCs were washed and plated in 96-well plates in triplicates (1×10^5 cells/well). The responder cells (5×10^4 cells/well) used for each assay were the NK T cell hybridomas 3C3, 1-2, and 1-4 (*30*), all of which have the invariant Vα14-Jα281 rearrangement characteristic of NK T cells. Antigen-dependent IL-2 production was measured after 16 hours of stimulation by enzyme-linked immunosorbent assay (ELISA).
16. M. Harata *et al.*, *Liver* **17**, 244 (1997).
17. When APCs were pulsed with glycolipids before the addition of CMA, there was only a slight increase in presentation of Gal(α1→2)GalCer relative to when CMA is added first. However, α-GalCer and Gal(α1→6)GalCer were presented at nearly the same level as the control (antigen only) when they were added before CMA, demonstrating that the more potent CMA can block antigen uptake and lysosome function.
18. A. J. Lusis, K. Paigen, *Biochim. Biophys. Acta* **437**, 487 (1976).
19. N. Asano *et al.*, *Med. Chem.* **37**, 3701 (1994).
20. N. Asano *et al.*, *Eur. J. Biochem.* **248**, 296 (1997).
21. F. Yagi *et al.*, *Arch. Biochem. Biophys.* **280**, 61 (1990).
22. R. O. Brady *et al.*, *N. Engl. J. Med.* **276**, 1163 (1967).
23. T. Ohshima *et al.*, *Proc. Natl. Acad. Sci. U.S.A.* **94**, 2540 (1997).
24. In preliminary studies, a CD1d/α-GalCer tetramer-based analysis of splenocytes in α-Gal $A^{-/-}$ mice revealed a 50% reduction in NK T cells. This reduction in number was associated with a sixfold reduction in the amount of α-GalCer–dependent IL-4 production by α-Gal $A^{-/-}$ splenocytes relative to wild-type splenocytes.
25. In three independent experiments, these GSLs were not antigenic when used as ligands with CD1d-coated plates to stimulate the 1-2 and 3C3 hybridomas (*12*).
26. Supplementary material is available at www.sciencemag.org/cgi/content/full/291/5504/664/DC1.
27. K. Sandhoff, T. Kolter, *Trends Cell Biol.* **6**, 98 (1996).
28. Lysosomes from A20 cells were isolated by ultracentrifugation of a light mitochondrial fraction containing 20% Optiprep (iodixanol) according to the manufacturer's instructions (Accurate Chemical , San Diego, CA). The lysosomes were sonicated and spectrophotometrically assayed for α-Gal A activity with *p*-nitrophenyl-α-D-galactoside.
29. A. Glithero *et al.*, *Immunity* **10**, 63 (1999).
30. L. Brossay *et al.*, *J. Immunol.* **160**, 3681 (1998).
31. Cells were fixed, permeabilized, and incubated with 10% donkey serum before the addition of the antibodies as previously described (*30*). CD1d molecules were labeled with biotinylated antibody (BD PharMingen, San Diego, CA), followed by streptavidin conjugated to Texas Red (Jackson Immunoresearch, West Grove, PA). The immunofluorescently labeled cells were analyzed with a Bio-Rad MRC 1024 ES laser scanning confocal microscope and the ×60 objective lens.
32. Gal(α1-2)GalCer–dependent IL-4 production by splenocytes was reduced 20-fold by DGJ treatment.

33. We thank R. Molyneux from the USDA Western Regional Research Center in Albany, CA, for the gift of calystegine C1. We also thank L. Gapin and J. Matsuda for critical reading of the manuscript and S. Levery, J. Backstrom, and C. Benedict for helpful discussions. This work was supported by NIH grants AI40617 and CA52511 to M.K. and a Career Development Award from the Crohn's and Colitis Foundation of America to D.E. This is manuscript number 381 of the La Jolla Institute for Allergy and Immunology.

25 July 2000; accepted 15 December 2000

Nucleotide-Dependent Single- to Double-Headed Binding of Kinesin

Kenji Kawaguchi[1] and Shin'ichi Ishiwata[1,2,3,4]*

The motility of kinesin motors is explained by a "hand-over-hand" model in which two heads of kinesin alternately repeat single-headed and double-headed binding with a microtubule. To investigate the binding mode of kinesin at the key nucleotide states during adenosine 5′-triphosphate (ATP) hydrolysis, we measured the mechanical properties of a single kinesin-microtubule complex by applying an external load with optical tweezers. Both the unbinding force and the elastic modulus in solutions containing AMP-PNP (an ATP analog) were twice the value of those in nucleotide-free solution or in the presence of both AMP-PNP and adenosine 5′-diphosphate. Thus, kinesin binds through two heads in the former and one head in the latter two states, which supports a major prediction of the hand-over-hand model.

Kinesin is a molecular motor that transports membrane-bound vesicles and organelles toward the plus end of a microtubule in various cells including neurons (*1*, *2*). Kinesin takes hundreds of 8-nm steps (the size of tubulin heterodimers composed of α and β subunits) (*3*–*5*) before detachment, so that the run length reaches longer than 1 μm (*3*, *6*). Each step is associated with one cycle of ATP hydrolysis (*7*, *8*). Structural and biophysical evidence shows that stepping of kinesin is triggered by conformational changes in the ATP-bound head (*9*).

A "hand-over-hand" model has been proposed to explain the processive movement of kinesin (Fig. 1) (*5*, *9*–*16*). To substantiate the hand-over-hand model, it is essential to determine the binding mode—either single- or double-headed binding—at each nucleotide state, and the kinetic step at which the transi-

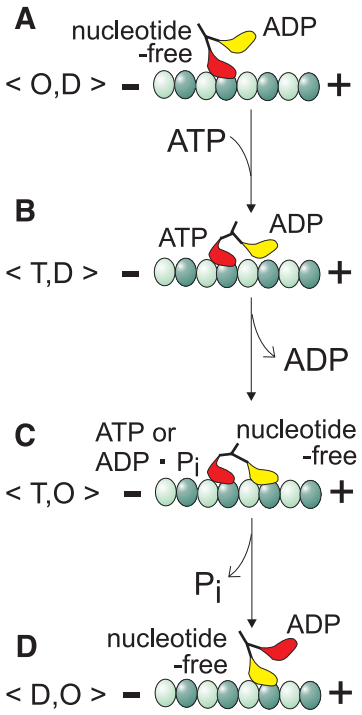

Fig. 1. A simplified version of the hand-over-hand model on the mechanism of kinesin motility proposed to date (*5*, *9*–*16*). O: nucleotide-free; D, T, and P_i: ADP, ATP, and inorganic phosphate, respectively.

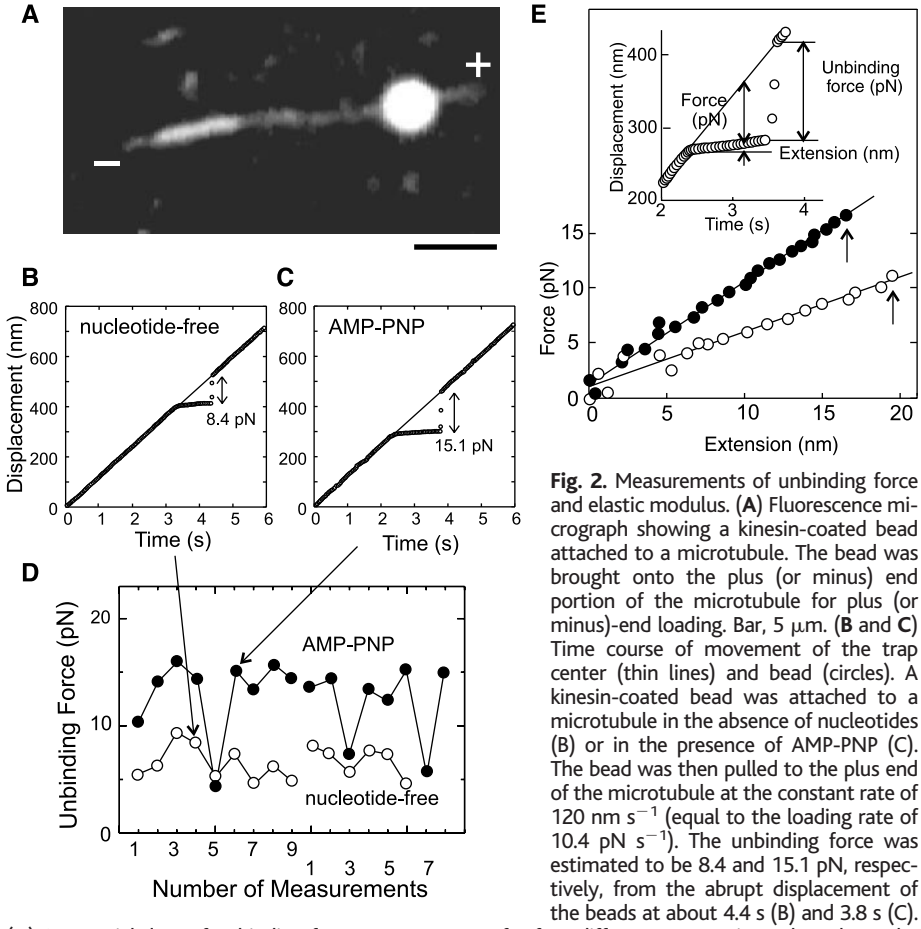

Fig. 2. Measurements of unbinding force and elastic modulus. (**A**) Fluorescence micrograph showing a kinesin-coated bead attached to a microtubule. The bead was brought onto the plus (or minus) end portion of the microtubule for plus (or minus)-end loading. Bar, 5 μm. (**B** and **C**) Time course of movement of the trap center (thin lines) and bead (circles). A kinesin-coated bead was attached to a microtubule in the absence of nucleotides (B) or in the presence of AMP-PNP (C). The bead was then pulled to the plus end of the microtubule at the constant rate of 120 nm s^{-1} (equal to the loading rate of 10.4 pN s^{-1}). The unbinding force was estimated to be 8.4 and 15.1 pN, respectively, from the abrupt displacement of the beads at about 4.4 s (B) and 3.8 s (C). (**D**) Sequential data of unbinding force measurements for four different preparations; data shown by arrows were taken from (B) and (C). Conditions: (B) and (○) in (D), nucleotide-free; (C) and (●) in (D), + AMP-PNP. (**E**) Examples of the force-extension relation (○, nucleotide-free; ●, + AMP-PNP). The relation was obtained from the time course of bead displacement as shown in the inset. To be strict, the force means the force component parallel to the glass surface, and the extension means the displacement of the bead in parallel to the glass surface (*27*). Arrows show the position of unbinding.

tion between the two binding modes occurs (*5*, *9*–*16*). Results of image analysis by cryo-electron microscopy on the dimeric kinesin-microtubule complex have been inconclusive; either single-headed (*13*, *14*) or double-headed (*15*, *16*) binding has been found to predominate both in the absence of nucleotides and in the presence of AMP-PNP. In solution the binding stoichiometry of the kinesin head and the tubulin heterodimer in a microtubule has a molar ratio of 2:1 in both the nucleotide-free state (*17*–*19*) and in the presence of AMP-PNP (*17*), implying a single-headed binding. In these studies, the microtubule was fully decorated by kinesin so that the conformation of kinesin may have been constrained (*16*). The intramolecular interhead distance of kinesin in the crystal structure is about 5 nm (*20*), considerably shorter than the size of the tubulin heterodimer. The kinetics of detachment in solution also suggests the single-headed binding not only in the nucleotide-free condition but also in the coexistence of AMP-PNP and adenosine 5′-diphosphate (ADP) (*21*). Overall, the evidence for the model remains indirect.

To obtain direct evidence for the binding mode at each nucleotide state, we measured the mechanical properties of single kinesin molecules attached to a microtubule in three different solvent conditions (*22*): in the absence of added nucleotides, in the presence of 0.5 mM AMP-PNP and 1 mM ADP, and in the presence of 1 mM AMP-PNP. The first condition corresponds to the ⟨O, O⟩ or ⟨O, D⟩ states (Fig. 1). Although apyrase was added, some proportion of heads may still have bound ADP because the kinesin was purified in the presence of ADP and the detachment rate of ADP is slow (*18*, *19*). The second condition mimics the ⟨T, D⟩ state. Under this condition, only one of the two heads is expected to bind AMP-PNP, while the other head is in the ADP state (*21*). The third condition is considered to represent the ⟨T, O⟩ state (*23*), because the binding ratio of AMP-PNP to kinesin molecules is reported to be 1:1 under the present condition (*23*).

An external load was imposed on a single kinesin-microtubule bead complex (Fig. 2A) (*24*, *25*) as it was moved toward the plus (or minus) end of a microtubule with optical tweezers (*26*, *27*). We repeated unbinding force measurements at nearly the same position on the same microtubule several times for the same bead, presumably for the same kinesin molecule (Fig. 2, B to D). Upon loading toward the plus end, unbinding force in the absence of nucleotides was about 7 pN (Fig. 2D), whereas that in the presence of AMP-PNP could apparently be classified into two components at about 14 pN (major) and 7 pN (minor), the latter corresponding to that in the absence of nucleotides. Using the same data, we obtained the force-extension relation on the kinesin-microtubule complex (Fig. 2E). This relation was almost linear, so that the elastic modulus could be estimated simply from the slope. The elastic modulus could also be classified into two components (compare Figs. 2E and 3, D to F). On the minus-end loading, the unbinding force for both components increased by 45% irrespective of the nucleotide states, keeping the elastic modulus unchanged. This shows that the binding is unstable

[1]Department of Physics, School of Science and Engineering; [2]Advanced Research Institute for Science and Engineering; [3]Materials Research Laboratory for Bioscience and Photonics, Waseda University, 3-4-1 Okubo, Shinjuku-ku, Tokyo 169-8555, Japan. [4]Core Research for Evolutional Science and Technology (CREST), "Genetic Programming" Team 13, Nogawa 907, Miyamae-ku, Kawasaki 216-0001, Japan.

*To whom correspondence should be addressed. E-mail: ishiwata@mn.waseda.ac.jp

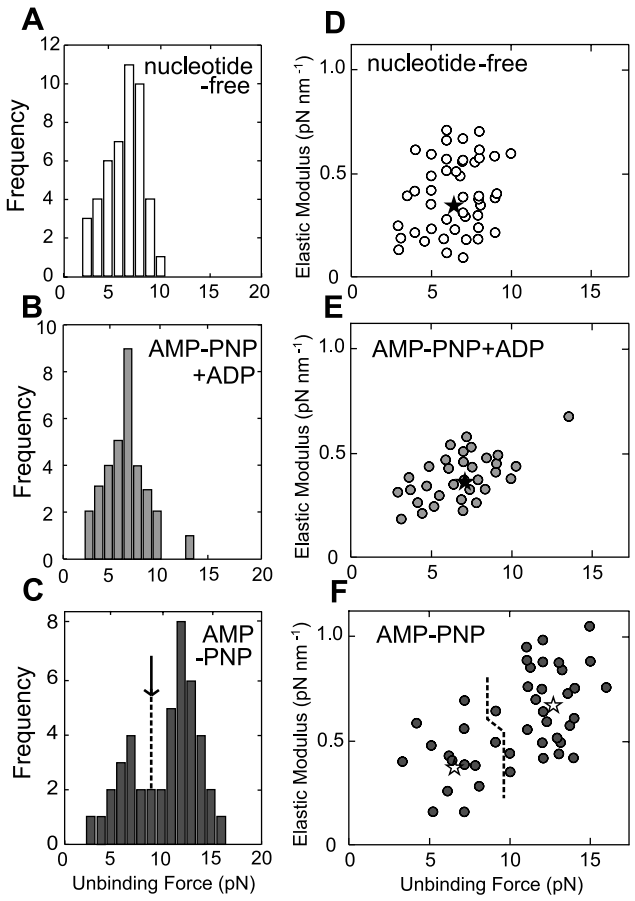

Fig. 3. Distribution of unbinding force (**A** to **C**) and relation between elastic modulus and unbinding force (**D** to **F**) at different nucleotide-binding states. The external load was applied toward the plus end. (A and D) Nucleotide-free (n = 46); (B and E) AMP-PNP + ADP (n = 33); (C and F) + AMP-PNP (n = 43). Unbinding force (pN) ± SD: 6.7 ± 1.8 (A), 7.2 ± 2.0 (B), and 6.6 ± 1.7 (n = 14), 12.8 ± 1.6 (n = 29) (C). Elastic modulus (pN nm^{-1}) ± SD: 0.35 ± 0.14 (D), 0.37 ± 0.16 (E), and 0.39 ± 0.17 (n = 14), 0.67 ± 0.21 (n = 29) (F). Loading rate (pN s^{-1}): 3.5 (A and D), 6.0 (B and E), and 4.3 (C and F). A single Gaussian distribution could simulate unbinding force distribution in (A) and (B). In contrast, the unbinding force distribution in (C) was simulated by the sum of two Gaussian distributions, with S- and L-components defined as the smaller and larger unbinding force, respectively. The boundary between the S- and L-components was determined by the junction of two Gaussian distributions [shown by an arrow (C)]; the boundary in (F) was determined according to that in (C). The average values for S- and L-components are shown by asterisks in (D) to (F).

for the plus-end loading compared with the minus-end loading.

The small (~7 pN; S-) and large (~14 pN; L-) components of unbinding force, respectively, correspond to those of the elastic modulus (Fig. 3). The finding that the unbinding force and the elastic modulus for the L-component were twice those for the S-component strongly suggests that the S- and L-components are attributable to the single- and double-headed binding of kinesin, respectively. Thus, each kinesin head contributes equally to the elastic modulus, such that each head equally shares the external load.

This interpretation shows that the binding mode in the ⟨O, D⟩ state (Fig. 1A) is single-headed. Assuming that AMP-PNP is an ATP analog, single-headed binding is also predominant in the ⟨T, D⟩ state (Fig. 1B). It is highly probable that the attached head binds AMP-PNP (ATP) (*9*), whereas the detached head binds ADP (*9*, *21*), because the attachment of the ADP-bound head was reported to be weak (*17*). In the ⟨T, O⟩ state (Fig. 1C), in contrast, double-headed binding is predominant. Here we find that, based on the bimodal distributions of unbinding force and elastic modulus at one loading rate (Figs. 2D and 3, C and F), both single- and double-headed binding exist. Additionally, we find that the proportion of the S-component decreased as the loading rate increased from 2 to 18 pN s^{-1} and, finally, disappeared at the highest loading rate we examined (18 pN s^{-1}), irrespective of the loading direction. This implies that double-headed binding predominates in the absence of external load. The finding that the unbinding force for the plus-end loading was smaller than that for the minus-end loading suggests that, in the "bridge" structure of double-headed binding (see Fig. 1C), the rear head is relatively unstable so that it tends to be detached. Such an asymmetry for the loading direction regarding the stability of the attached state is favorable for kinesin motors stepping forward.

References and Notes

1. R. D. Vale, in *Guidebook to the Cytoskeletal and Motor Proteins*, T. E. Kreis, R. D. Vale, Eds. (Oxford Univ. Press, Oxford, ed. 2, 1999), pp. 398–402.
2. N. Hirokawa, *Science* **279**, 519 (1998).
3. S. M. Block *et al.*, *Nature* **348**, 348 (1990).
4. K. Svoboda *et al.*, *Nature* **365**, 721 (1993).
5. J. Howard, *Annu. Rev. Physiol.* **58**, 703 (1996).
6. K. Kawaguchi, S. Ishiwata, *Biochem. Biophys. Res. Commun.* **272**, 895 (2000).
7. W. Hua *et al.*, *Nature* **388**, 390 (1997).
8. M. J. Schnitzer, S. M. Block, *Nature* **388**, 386 (1997).
9. S. Rice *et al.*, *Nature* **402**, 778 (1999).
10. R. D. Vale, R. A. Milligan, *Science* **288**, 88 (2000).
11. E. Mandelkow, K. A. Johnson, *Trends Biochem. Sci.* **23**, 429 (1998).
12. D. D. Hackney, *Proc. Natl. Acad. Sci. U.S.A.* **91**, 6865 (1994).
13. K. Hirose *et al.*, *Mol. Biol. Cell* **10**, 2063 (1999).
14. I. Arnal, R. H. Wade, *Structure* **6**, 33 (1998).
15. M. Thormählen *et al.*, *J. Mol. Biol.* **275**, 795 (1998).
16. A. Hoenger *et al.*, *J. Mol. Biol.* **297**, 1087 (2000).
17. A. Lockhart, I. M. Crevel, R. A. Cross, *J. Mol. Biol.* **249**, 763 (1995).
18. Y. Z. Ma, E. W. Taylor, *J. Biol. Chem.* **272**, 724 (1997).
19. S. P. Gilbert, M. L. Moyer, K. A. Johnson, *Biochemistry* **37**, 792 (1998).
20. F. Kozielski *et al.*, *Cell* **91**, 985 (1997).
21. Y. Vugmeyster, E. Berliner, J. Gelles, *Biochemistry* **37**, 747 (1998).
22. Kinesin and tubulin were prepared from bovine (*25*) and porcine (*28*) brains, respectively. Polarity-marked microtubules labeled with tetramethylrhodamine succinimidyl ester (Molecular Probes, Eugene, OR) were prepared according to Hyman (*28*) except that tubulin was not treated with *N*-ethylmaleimide (NEM) (Fig. 2A). Kinesin-coated beads and the flow cell were prepared as described (*6*, *25*). The final solvent condition was ~0.1 pM kinesin-coated beads, 2 mM $MgCl_2$, 80 mM Pipes (pH 6.8), 1 mM EGTA, 0.7 mg ml^{-1} filtered casein, 1 U ml^{-1} apyrase (nucleotide-free condition), 0.5 mM AMP-PNP with 1.0 mM ADP (AMP-PNP + ADP condition) (*21*) or 1 mM AMP-PNP (+ AMP-PNP condition), 10 μM taxol, 10 mM dithiothreitol, and an oxygen-scavenging enzyme system (*6*). All experiments were performed at 25° ± 1°C.
23. B. J. Schnapp *et al.*, *Proc. Natl. Acad. Sci. U.S.A.* **87**, 10053 (1990).
24. K. Svoboda, S. M. Block, *Cell* **77**, 773 (1994).
25. H. Kojima *et al.*, *Biophys. J.* **73**, 2012 (1997).
26. T. Nishizaka *et al.*, *Nature* **377**, 251 (1995).
27. A microscopy system equipped with optical tweezers was as previously described (*26*); the stiffness of the optical trap was estimated to be 0.087 pN nm^{-1}. The bead in the medium was first trapped by optical tweezers and placed in contact with a microtubule for 20 to 30 s, a period considered sufficient to realize the binding equilibrium between kinesin molecule and a microtubule. The trap center was then moved at a constant rate to the plus (or minus) end of the microtubule (Fig. 2A) until the unbinding event occurred. With a single-molecule attachment between the bead and the microtubule, it is possible for the bead to move some distance relative to the microtubule without deviating from the trap center. This is mainly because of the rotational movement of the bead in the trap. This rotational movement is not registered on the position detector. As observed in Fig. 2, B and C, for the first part of the movement of the bead, the kinesin may be attached to the microtubule but does not show in the displacement until the bead-kinesin-microtubule link pulls tight. On the basis of the size and geometry of the kinesin-tethered bead (*24*) (radius of bead, 0.5 μm; length of kinesin, 60 nm), we can estimate that the largest displacement required before the external load is imposed for the unbinding event is ~600 nm. In fact, this displacement was as large as 300 ± 140 nm (n = 122). Also, the actual extension of kinesin is estimated to be 8.3 ± 1 nm (Fig. 2E), which is approximated by 18 nm × cos(θ), where θ (1.1 ± 0.1 rad) is the angle between the kinesin tether and the glass surface. In our bead assay, the external force responsible for the extension of the kinesin-microtubule complex should also be multiplied by cos(θ). Thus, the elastic modulus is kept unchanged.
28. A. A. Hyman, *J. Cell Sci.* **s14**, 125 (1991).

29. We thank K. Kinosita Jr. and T. Nishizaka for continuous collaboration. We are grateful to Y. Y. Toyoshima and T. Yagi for suggestions on the preparation of kinesin and tubulin, and to H. Higuchi for the protocol for kinesin bead assay. We also thank J. Howard, K. Hirose, and W. Rozycki for critical reading of the manuscript. This research was partly supported by Grants-in-Aid for Scientific Research, for Scientific Research on Priority Areas, and for the High-Tech Research Center Project from the Ministry of Education, Science, Sports, and Culture of Japan; by Grants-in-Aid from CREST; and by the Mitsubishi Foundation.

28 September 2000; accepted 18 December 2000